03,16

The Nature of Interface Recombination in Heterostructures Based on InAsSb(P) Solid Solutions

© I.D. Kirilenko[1], V.V. Romanov[2], N.L. Bazhenov[2], I.N. Trapeznikova[2], K.D. Mynbaev[2], K.D. Moiseev[2]

[1] ITMO University,
St. Petersburg, Russia
[2] Ioffe Institute,
St. Petersburg, Russia
E-mail: idkirilenko@itmo.ru

Received December 13, 2025
Revised December 13, 2025
Accepted December 15, 2025

Studies of optical transmittance and electroluminescence of heterostructures based on InAsSb(P) solid solutions were performed. Transmittance spectra investigation revealed the dependence of charge carrier concentration in the narrow-gap layer $InAs_{1-y}Sb_y$ on InSb fraction y. It was shown that the increase of charge carrier concentration localized in potential wells at the heterointerface InAsSb/InAsSbP leads to the strong dipole formation, which makes interface transitions the prevalent channel of radiative recombination in such narrow-gap heterostructures.

Keywords: InAsSb(P), optical transmittance, electroluminescence, interface transitions.

DOI: 10.61011/PSS.2026.01.63332.346-25

1. Introduction

Gas spectroscopy, chemical detection and environmental monitoring systems, as well as medical diagnostics are currently the main applications of sensors based on semiconductor structures operating in the mid-infrared (IR) wavelength range [1–5]. A narrow-gap solid solution (SS) of $InAs_{1-y}Sb_y$ can be used as an emissive layer in such structures, in which the band gap width E_g can be varied by changing the content of InSb to cover the spectral range from 3.5 to 11.0 μm at a room temperature. However, the design and fabrication of optoelectronic and photoelectronic devices operating effectively in the IR spectral range at high temperatures is hindered by the predominance of nonradiative recombination processes of charge carriers over radiative ones in narrow-gap semiconductors. Therefore, identifying possible recombination channels and studying their effect on the spectral and optical characteristics of narrow-gap heterostructures (HSs) remains a key challenge, as the energy band diagram of the HSs varies with the chemical composition of the constituent semiconductors.

Previously, we investigated the recombination processes in narrow-gap LED HS $InAs/InAs_{1-y}Sb_y/InAsSbP$ with InSb content in the emissive layer of up to $y = 0.16$ [6,7]. These studies focused on the nature of long-wavelength (up to 5.1 μm at a temperature of $T = 300$ K) electroluminescence (EL). Given the temperatures below 100 K, a second short-wavelength radiation band attributed to recombination in the substrate was also observed in the EL spectra of the HSs. Later, it was shown that the specific features of InAsSb/InAsSbP heterointerface formation, caused by the lattice mismatch between the emissive and barrier layers, as well as the peculiarities of quaternary InAsSbP SS deposition onto the ternary InAsSb SS epitaxial layer using metalorganic vapor phase epitaxy (MOVPE), can lead to the formation of a type-II heterojunction even in HSs with a relatively low InSb content (up to $y = 0.06$) in the emissive layer [8,9]. This provides additional ways for tuning the emission wavelength in such structures, while the presence of two recombination channels in them may be of interest for achieving dual-wavelength EL (at both reference and operating wavelengths) within a single HS [10]. This approach allows minimizing the device dimensions and improving its efficiency by incorporating several radiative recombination channels in spatially separated regions of a single HS. Ensuring the stable operation of such a device requires the consistency of the recombination channels to prevent spontaneous switching between them triggered by shifts in operating conditions (e.g., temperature fluctuations or changes in the bias voltage). Hitherto, this issue has been insufficiently addressed in the literature. This paper investigates the nature of charge carrier recombination in single and double n-InAs/(n-$InAs_{1-y}Sb_y$)/p-InAsSbP HSs of various designs. The studies were conducted over a wide range of temperatures and bias voltages, and the observed effects were compared with the features of the energy band diagrams of HSs.

2. Experimental procedure

Experimental samples were grown by MOVPE in a horizontal reactor at atmospheric pressure; the growth process details are discussed in Ref. [11]. Undoped n^0-InAs(001) wafers with an electron concentration of $n \sim 10^{16}$ cm^{-3} at $T = 300$ K were used as substrates. The $InAs_{1-y}Sb_y$

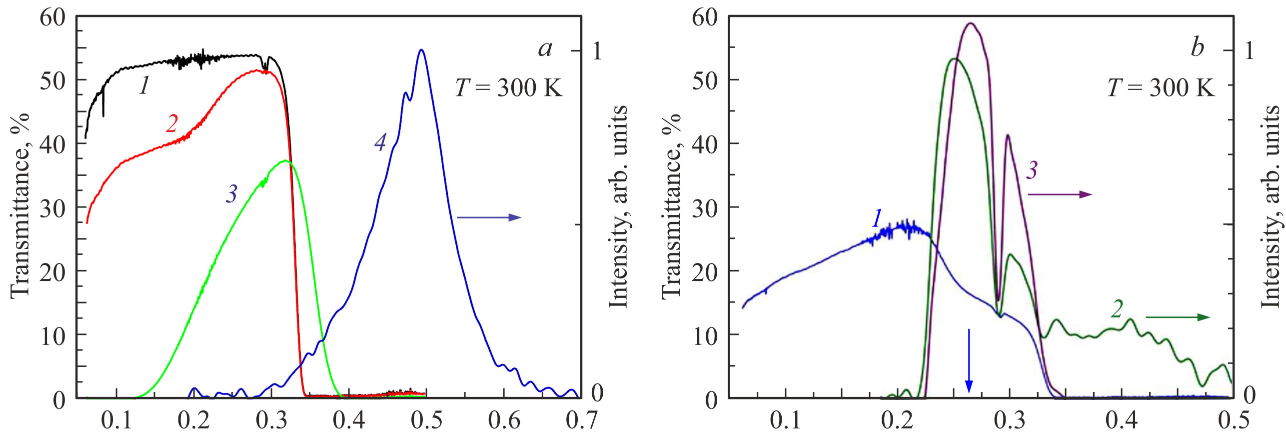

Figure 1. (*a*) OT spectra of the substrate n^0-InAs (*1*), sample *C* (*2*), structure n^+-InAs:S/n^0-InAs (*3*), the PL spectrum of the barrier layer for sample *C* from Ref. [9] (*4*). (*b*) For sample *G*: OT spectrum (*1*), PL spectrum from [9] (*2*), EL from [14] (*3*), the blue arrow indicates E_g of the ternary solid solution of sample *G*.

Studied samples

Label of sample	Sample structure
B	n^0-InAs/n^0-InAs$_{0.85}$Sb$_{0.05}$P$_{0.10}$
C	n^0-InAs/p^+-InAs$_{0.31}$Sb$_{0.22}$P$_{0.47}$:Zn
D	n^0-InAs/p^+-InAs$_{0.94}$Sb$_{0.06}$:Zn
E	n^0-InAs/n^0-InAs$_{0.92}$Sb$_{0.08}$/p^+-InAs$_{0.32}$Sb$_{0.26}$P$_{0.42}$:Zn
F	n^0-InAs/n^0-InAs$_{0.91}$Sb$_{0.09}$/p^+-InAs$_{0.34}$Sb$_{0.25}$P$_{0.41}$:Zn
G	n^0-InAs/n^0-InAs$_{0.88}$Sb$_{0.12}$/p^+-InAs$_{0.32}$Sb$_{0.29}$P$_{0.39}$:Zn

epitaxial layers in the double HSs (samples E, F, G, see table) were not intentionally doped, yet exhibited *n*-type conductivity. The InAs$_{1-x-y'}$Sb$_{y'}$P$_x$ SS with a predefined solid-phase composition of $y' = 0.22$ and $x = 0.47$ was used to grow the top epitaxial layer. During growth process, this layer was doped with Zn to achieve *p*-type conductivity. The layer structure of the HSs, including the actual values of y' and x, is presented in the table.

For EL measurements, the chips were fabricated and mounted (soldered) onto TO-18 headers from the substrate side, the emission was collected from the epitaxial layer side. The EL spectra were recorded under pulsed excitation (frequency of $f = 1$ kHz and a pulse duration of $\tau = 2\,\mu$s), using a cooled InSb photodiode. Optical transmittance (OT) spectra were recorded at $T = 300$ K using a Shimadzu FTIR-8400S Fourier spectrometer.

3. Experimental results and discussion

The OT spectrum of the undoped n^0-InAs substrate (Figure 1, *a*, spectrum *1*) exhibits a sharp high-energy (HE) edge in the region of photon energies close to $E_{g,\mathrm{InAs}}$. Notably, the transmittance is cut off at photon energy of ~ 0.340 eV, which is 14 meV lower than $E_{g,\mathrm{InAs}} = 0.354$ eV at $T = 300$ K [12]. The presence of an epitaxial layer with a bandgap E_g wider than that of InAs (for example, an InAsSbP layer with $E_{g,\mathrm{InAsSbP}} \sim 0.5$ eV at $T = 300$ K) within the HS does not affect the HE edge of the entire HS spectrum, since the radiation with photon energies $h\nu > E_{g,\mathrm{InAs}}$ is completely absorbed in the n^0-InAs substrate. Nevertheless, within the energy range of 0.1–0.2 eV, a significant drop in transmittance is observed, while the rest of the spectrum (0.25–0.34 eV) shows virtually no attenuation. The observed drop in transmittance is most likely due to free-carrier absorption in the HS bulk, which arises from epitaxial growth inhomogeneities, structural defects, and interface recombination at the heterointerface. The same figure also shows the OT spectrum of the structure n^+-InAs:S/n^0-InAs grown on a heavily doped substrate with $n^+ \sim 2 \cdot 10^{18}$ cm^{-3} (Figure 1, *a*, spectrum *3*). The HE edge of this spectrum shows a shift towards higher photon energies by ~ 40 meV relative to the edge for an undoped substrate, which is explained by the position of the Fermi level in the conduction band of a highly doped semiconductor. In addition, radiation with $h\nu < 0.150$ eV is intensively absorbed in the volume of a highly doped substrate. Presumably, this feature of OT spectra is also related to the absorption of radiation by free carriers. Thus, the low-energy (LE) edge of the spectra reflects the doping level of the compounds forming this HS.

The introduction of an additional epitaxial layer in the form of a ternary SS InAsSb with E_g lower than that of InAs into the studied HS modifies the main part of the OT spectrum. Thus, there is a pronounced decrease in signal intensity near $h\nu = 0.264$ eV in the OT spectrum of the sample *G* (Figure 1, *b*, spectrum *1*), which can be explained by radiation absorption in the volume of the InAs$_{0.88}$Sb$_{0.12}$ layer. The obtained photon energy value is close in magnitude to E_g of the narrow-gap layer [13], and also corresponds to the spectral position of the photoluminescence band maximum (Figure 1, *b* spectrum *2* [9])

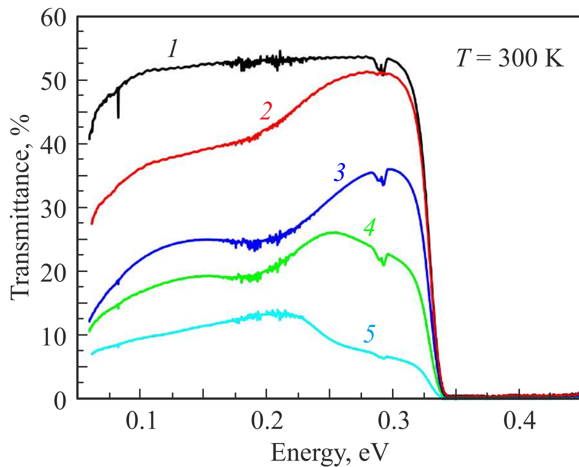

Figure 2. OT spectra of the substrate n^0-InAs (*1*), sample *C* (*2*), as well as samples: *D*, $y = 0.06$ (*3*), *E*, $y = 0.08$ (*4*), *G*, $y = 0.12$ (*5*).

and EL band maximum (Figure 1, *b* spectrum *3* [14]). The doping level of the *n*-InAsSb layer can be estimated by comparing the OT spectra for the n^+-InAs : S/n^0-InAs structure and *G* sample. The concentration of residual electrons in the $InAs_{0.88}Sb_{0.12}$ SS grown by MOVPE was $n_{SS} \sim 6 \cdot 10^{17}\,\text{cm}^{-3}$.

The presence of a layer with a higher concentration of free carriers than in an undoped substrate directly affects the shape of the LE edge of the OT spectrum (Figure 2). It should be noted that the InAsSbP layers are isomorphic with the InAs substrate and have a slight deviation in the crystal lattice parameter. As a result, when the quaternary SS is deposited on the InAs substrate, structural defects are formed in low concentrations. The InAsSbP epitaxial layer exhibits *p*-type conductivity due to doping with an acceptor impurity of Zn. A linear approximation of the drop in the OT signal in the region of low photon energies allows estimating the concentration of residual free carriers for the compensated layer p^+-InAsSbP : Zn, which is $p^+ \sim 2 \cdot 10^{17}\,\text{cm}^{-3}$.

The situation is different with the InAsSb layer. An elevation in the Sb content in the grown ternary SS leads to a higher lattice mismatch with the InAs substrate and the quaternary InAsSbP SS, and, consequently, an enhanced internal stresses, which, in turn, significantly increases the concentration of structural defects. It can be expected that the concentration of electrons rises in the narrow-gap *n*-type layer. Figure 2 shows how the LE edge of the OT spectra changes for HS, which contain layers of ternary SS n^0-$InAs_{1-y}Sb_y$ in the range of compositions $y = 0.06{-}0.12$. The shape of the spectra, as well as a general decrease in the intensity of the recorded signal, indicate an increase in the electron concentration in $InAs_{1-y}Sb_y$ n_{SS} from $3 \cdot 10^{17}$ to $6 \cdot 10^{17}\,\text{cm}^{-3}$, depending on its composition y. Since these SS were obtained under the same technological conditions, the increase of n_{SS} can be attributed to internal factors of the studied HS due to the defect density in the narrow-gap epitaxial layers.

In addition, the HS studied in this work had a sufficiently high potential barrier for electrons at the InAs(Sb)/InAsSbP heterointerface. According to the preliminary calculation in Ref. [15], the conduction band offset was $\Delta E_c = 0.2\,\text{eV}$. The presence of such a barrier can significantly affect the electrical and luminescent properties of the HS. Figure 3, *a* schematically shows the energy diagram of the HS n^0-InAs/n^0-$InAs_{0.91}Sb_{0.09}$/p^+-$InAs_{0.31}Sb_{0.22}P_{0.47}$: Zn in thermodynamic equilibrium at $T = 77\,\text{K}$, which was calculated in accordance with experimental data given in Ref. [15]. The InAsSb/InAsSbP heterojunction is of staggered type II with large energy offsets at the interface for conduction bands ΔE_c and relatively small valence bands offsets ΔE_v [16]. It is known that in a type II staggered heterojunction, self-consistent potential wells are formed on opposite sides of the heterointerface as a result of band bending. Charge carriers are confined in such wells by the electric field of the resulting dipole. An increase in the concentration of free electrons in the conduction band of the InAsSb narrow-gap layer in the presence of a potential barrier at the type II heterointerface leads to their localization near the heterointerface and an increase in the probability of interface radiative transitions across the InAsSb/InAsSbP interface (Figure 3, *b*).

When an external forward bias was applied to the InAs/InAsSb/InAsSbP HS under study (samples *F* and *G*), EL was detected at $T = 77\,\text{K}$, exhibiting two distinct bands (Figure 4): the HE band ($h\nu_2$) and the LE band ($h\nu_1$). The photon energy at the maximum of the emission band $h\nu_1$ varied depending on the composition of the narrow-gap HS layer, while the spectral position of the EL HE-band did not change ($h\nu_2 = 0.39\,\text{eV}$) and was close to $E_{g,\text{InAs}} = 0.408\,\text{eV}$ at $T = 77\,\text{K}$. The EL spectrum of sample *F* ($y = 0.09$) at the initial injection level was dominated by the band $h\nu_1$, and its intensity remained constant until a certain value of the pumping current (Figure 4, *a* and *c*), while the intensity of the band $h\nu_2$ increased over the entire range of current values. With a further increase in the injection level, a redistribution in the intensity of the EL bands was observed: the band $h\nu_1$ gradually decayed, and the band $h\nu_2$ became dominant. According to the energy diagram shown in Figure 3, *b*, the intensity of the band $h\nu_1$ decreased due to the leakage of holes from the potential well at the heterointerface. Under the action of an external electric field, more holes overcame the potential barrier, entering the InAsSb bulk and then the n^0-InAs substrate. As a result of the described redistribution of charge carriers, the probability of radiative transitions in the substrate increased, which was expressed in an increase in the intensity of the band $h\nu_2$.

The EL spectrum for sample *G* ($y = 0.12$) also consisted of two emission bands: the band $h\nu_1$ dominated the entire range of pumping currents, and the intensity of the band $h\nu_2$ increased slightly with current (Figure 4, *b* and *d*). In this sample, the main EL channel consisted of radiative

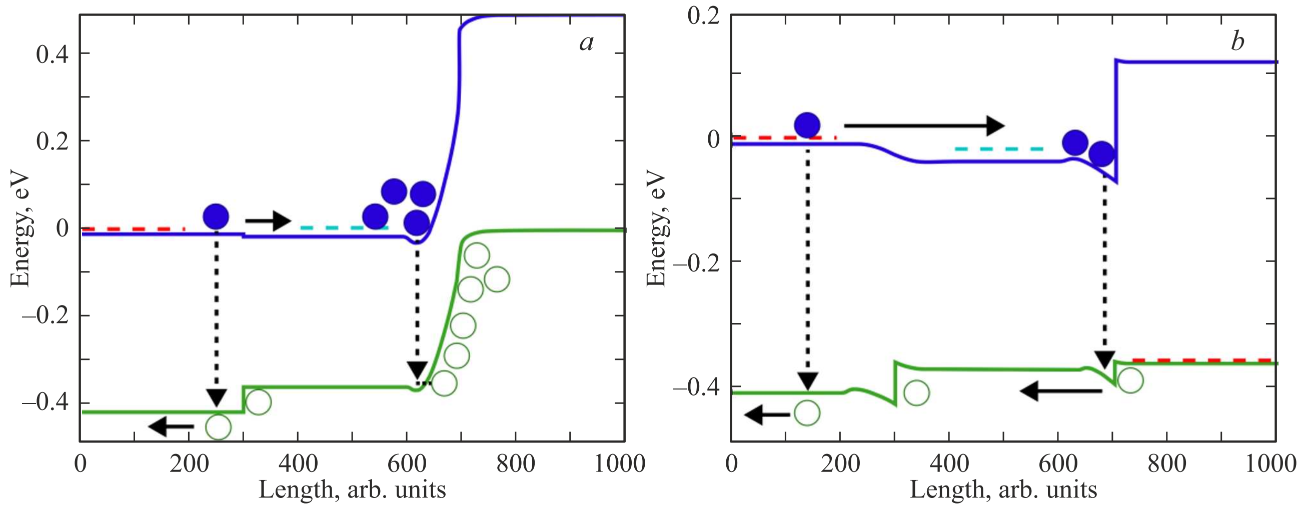

Figure 3. Energy diagrams ($T = 77\,\mathrm{K}$) of HS using the example of a structure with the value $y = 0.09$: under a minimal forward bias (a), at a forward bias of 0.35 V at the InAsSb/InAsSbP (b) heterojunction. For simplification, recombination transitions are shown as interband.

Figure 4. EL spectra of samples F (a) and G (b) at $T = 77\,\mathrm{K}$ and pumping currents, A: 0.4 (1), 1 (2), 2 (3) and 4 (4). The intensity of the EL bands $h\nu_1$ and $h\nu_2$ for samples F (c) and G (d).

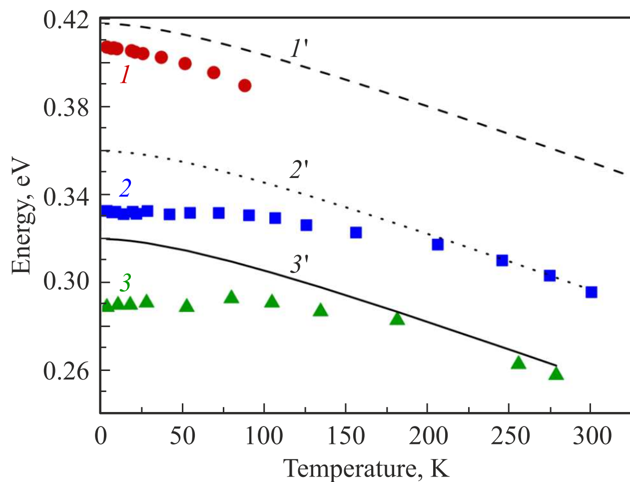

Figure 5. Temperature dependences of energy at the maximum of EL bands: EL band $h\nu_2$ common for samples F and G (symbols *1*) and calculated curve $E_{g,\text{InAs}}$(line *1′*); for sample F EL band $h\nu_1$ (symbols *2*) and calculated curve $E_{g,\text{InAsSb}}$ (*2′*); for sample G EL band $h\nu_1$ (symbols *3*) and the calculated curve $E_{g,\text{InAsSb}}$ (*3′*).

transitions near the InAsSb/InAsSbP heterointerface. The decrease in the potential barrier for electrons had no significant effect on the redistribution of carrier fluxes between the two described recombination channels, which indicates high concentrations of electrons and holes in potential wells at the type II heterointerface [17]. It is noteworthy that as the pump level increased, the maximum of the emission band $h\nu_1$ shifted in the direction of higher photon energies — the so-called „blue“ shift. A similar behavior of the EL bands can be observed when the Fermi quasi-levels for electrons and holes localized in the corresponding wells on the heterointerface shift in energy relative to each other during the filling of the wells.

It was previously shown that, depending on the composition of the narrow-gap layer, the type of heterojunction $InAs_{1-y}Sb_y$/InAsSbP changes [18]. As the Sb content in InAsSb increases, the type I heterojunction transforms into a type II heterojunction with a valence band offset at the SS interface sufficient to form a potential well and localize holes in it. An increase in the concentration of electrons on one side of the heterointerface in close proximity to it and an accumulation of holes on the opposite side lead to the formation of two charges of opposite signs creating a strong dipole, the electric field of which holds charges near the interface. The matrix element of the radiative transitions at the heterointerface increases significantly, which defines the interface transitions as the main channel of the EL. The weak temperature dependence of the low-energy radiation band for InAs/$InAs_{1-y}Sb_y$/InAsSbP heterostructures in the range of compositions $y = 0.09{-}0.12$ obtained at low temperatures indicates a strong localization of charge carriers near the type II heterostructure (Figure 5). An increase in temperature leads to delocalization of charge carriers in wells due to thermal activation, therefore, at $T > 170$ K, interband recombination in the InAsSb bulk becomes the dominant channel of radiative recombination due to leakage of holes from localization levels through the valence band offset at the heterointerface. A typical example of such radiative transitions is the EL high-energy band ($h\nu_2$), common to all studied HS. It demonstrates a pronounced temperature dependence, which coincides in shape with the calculated dependence curve $E_{g,\text{InAs}}(T)$, and corresponds to radiative transitions to impurity states with ionization energy $E_A \approx 12$ meV.

4. Conclusion

Optical transmission spectra were used to show the dependence of the concentration of free charge carriers in heterostructures based on InAsSb(P) solid solutions on the Sb content in the emissive layer of $InAs_{1-y}Sb_y$. An increase in y led to an increased mismatch in the crystal lattice parameter of the ternary solid solution with the substrate and with the quaternary solid solution, as a result, the density of structural defects increased. In turn, the high density of defects determined the increase in the concentration of free electrons in the ternary solid solution. As a result, a larger number of charges of opposite signs were localized in potential wells at the InAsSb/InAsSbP heterointerface, forming a strong dipole, which enabled interface transitions to become the main and stable channel of long-wave radiative recombination. The presence of a second, short-wave channel on the InAs/InAsSb heterointerface makes it possible to implement an emitter with two operating wavelengths.

Conflict of interest

The authors declare that they have no conflict of interest.

References

[1] G.F. Rangel, L.D. de Leon Martínez, L.S. Walter, B. Mizaikoff. Trends Anal. Chem. **180**, 117916 (2024).
[2] Y. Tang, Y. Zhao, H. Liu. ACS Sens. **7**, *12*, 3582 (2022).
[3] M. Hlavatsch, B. Mizaikof. Anal. Sci. **38**, 1125 (2022).
[4] W. Gawron, P. Madejczyk, P. Martyniuk, S. Krishna. IEEE Sens. J. **24**, *9*, 14151 (2024).
[5] H. Fujita, D. Yasuda, S. Ota, H. Geka, E. Gomes Camargo, S. Isshiki, T. Fukunaka, N. Kuze. IEEE Sens. Lett. **7**, *9*, 3502004 (2023).
[6] M.S. Ruzhevich. Rev. Adv. Mater. Technol. **3**, *4*, 24 (2021).
[7] A.A. Semakova, V.V. Romanov, N.L. Bazhenov, K.D. Mynbaev, K.D. Moiseev. Semiconductors **55**, *3*, 354 (2021).
[8] I.D. Kirilenko, M.S. Ruzhevich, N.L. Bazhenov, M.V. Tomkovich, V.V. Romanov, K.D. Moiseev, K.D. Mynbaev. Rev. Adv. Mater. Technol. **6**, *4*, 178 (2024).
[9] I.D. Kirilenko, M.S. Ruzhevich, V.V. Romanov, K.D. Moiseev, M.V. Dorogov, M.V. Tomkovich, D.D. Firsov, I.V. Chumanov, O.S. Komkov, K.D. Mynbaev. St. Petersburg State Polytechnical University Journal. Physics and Mathematics **18**, *1.1*, 105 (2025).

[10] M.M. Grigoryev, P.A. Alekseev, E.V. Ivanov, K.D. Moiseev. Semiconductors **47**, *1*, 28 (2013).
[11] V.V. Romanov, K.D. Moiseev. Phys. Solid State **65**, *10*, 1634 (2023).
[12] NSM Archive [Electronic source]: Physical Properties of Semiconductors. — Available at: http://www.matprop.ru/ (date of access 17.09.2025)
[13] V.V. Romanov, E.V. Ivanov, K.D. Moiseev. Phys. Solid State **61**, *10*, 1699 (2019).
[14] V.V. Romanov, I.A. Belykh, E.V. Ivanov, P.A. Alekseev, N.D. Il'inskaya, Yu.P. Yakovlev. Semiconductors **53**, *6*, 822 (2019).
[15] K.D. Moiseev, V.V. Romanov. Phys. Solid State **63**, *4*, 595 (2021).
[16] M.M. Grigoryev, E.V. Ivanov, K.D. Moiseev. Semiconductors **45**, *10*, 1334 (2011).
[17] K.D. Moiseev, M.P. Mikhailova, Yu.P. Yakovlev. Semiconductors **37**, *8*, 985 (2003).
[18] V.V. Romanov, K.D. Moiseev. Phys. Solid State **65**, *10*, 1634 (2023).

Translated by A.Akhtyamov